Journal of Magnetic Resonance 196 (2009) 23–32

Contents lists available at ScienceDirect

Journal of Magnetic Resonance

journal homepage: www.elsevier.com/locate/jmr

IRIS-HSVD algorithm for automatic quantitation of *in vivo* ^{31}P MRS

Xin Wang [a], Jing-Huei Lee [a,b,*]

[a] Department of Biomedical Engineering, P.O. Box 670586, University of Cincinnati, 231 Albert Sabin Way, Room 6153A, MSB, Cincinnati, OH 45267, USA
[b] Center for Imaging Research, P.O. Box 670583, University of Cincinnati, Cincinnati, OH 45267, USA

ARTICLE INFO

Article history:
Received 10 March 2008
Revised 26 September 2008
Available online 30 September 2008

Keywords:
Magnetic resonance spectroscopy
Quantification
Hankel singular value decomposition
Iteration
Automation
^{31}P

ABSTRACT

The rapid development of ^{31}P magnetic resonance spectroscopy (MRS) has enhanced non-invasive measurement of brain metabolites, which is important for biomedical research. The accuracy and efficiency of data post processing and quantification is paramount for MRS applications. One of the difficulties with *in vivo* ^{31}P MRS data quantification is the separation of broad line-width resonances from chemical compounds' resonances under a low signal-to-noise ratio condition. Furthermore, the chemical shift of some compounds caused by pH and Mg^{2+} concentration can be troublesome. This work aims to develop an automatic algorithm using a state-space based quantification approach to solve the above mentioned problems. To achieve this aim, we utilized an HSVD based adaptive optimizing prior knowledge algorithm, which uses so called "interference" signals to optimize prior knowledge iteratively for parameter optimization. We termed this algorithm IRIS-HSVD, which stands for Iterative Reduction of Interference Signal HSVD. The Monte Carlo evaluations of the algorithm were conducted with simulated data using *in vivo* parameters commonly obtained from a 4 T scanner. The performance of this algorithm using simulated data was compared to those of other automatic methods including HSVD and HTLS-PK. Examples of *in vivo* ^{31}P data obtained from brains of healthy subjects on a 4T MRI scanner were also presented, which demonstrated the superiority of the new method. The results were compared with those using AMARES.

1. Introduction

Magnetic resonance spectroscopy (MRS) has become increasingly important in biomedical research because of its ability to measure *in vivo* biochemical information. Multi-voxel ^{31}P MRS is a useful tool for the study of *in vivo* energy metabolites in humans and animals [1,2]. However, spectral analysis can be tedious and time consuming, particularly for multi-voxel data acquired using 2D or 3D MRS. Additionally, it suffers from a low signal-to-noise ratio (SNR), spectral overlapping, chemical frequency variation influenced by a biophysiological environment, and significant baseline artifacts. These issues can be attributed to (1) a low natural concentration of ^{31}P biochemical compounds in *in vivo* samples, (2) the variation of certain ^{31}P resonances by the influence of physiological environment, (3) the origination of some signals from immobile compounds (presumably from bone marrow and/or cell membranes), and/or (4) imperfect hardware. These complications continue to challenge the development of an automatic algorithm for MRS data quantification, which is strongly needed to further advance this methodology to widespread clinical applications.

The algorithms developed for MRS data analysis based on the state-space approach are rapidly increasing due to significant improvements in quantitation robustness and accuracy [3]. The state-space methods often employ tools such as the Singular Value Decomposition (SVD) [4] or the orthogonal matrix triangularization (also known as QR decomposition) [5,6] to distinguish the signal and noise subspaces. Compared to the frequency domain methods [7], the state-space approach has less sensitivity to phase errors and greater tolerance of spectral overlap, baseline distortions and/or missing data samples [8,9].

The SVD, as well as its derivative methods such as Hankel SVD (HSVD) [10,11], Hankel Lanczos SVD (HLSVD) [12] and Linear Prediction SVD (LPSVD) [13,14], provide nearly automatic quantification approaches, although their results are often prone to lack of physical and/or physiological meaning (i.e., specificity and accuracy). It was demonstrated that the accuracy of these approaches can be improved by introducing Hankel Total Least Squares (HTLS) techniques [15]. Furthermore, incorporating prior knowledge with subspace methods (or, in general, any methods) could further improve performance robustness. For example, simulated spectra by spin physics were utilized to obtain a theoretical estimation of the frequencies and damping factors of targeted resonances in QUEST (quantitation based on quantum estimation), which can also handle baseline distortions [16]. Prior knowledge of signal frequencies and damping factors can also serve as the starting

* Corresponding author. Address: Department of Biomedical Engineering, P.O. Box 670586, University of Cincinnati, 231 Albert Sabin Way, Room 6153A, MSB, Cincinnati, OH 45267, USA. Fax: +1 513 558 7164.
E-mail address: jing-huei.lee@uc.edu (J.-H. Lee).

1090-7807/$ - see front matter © 2008 Elsevier Inc. All rights reserved.
doi:10.1016/j.jmr.2008.09.024

estimation values in AMARES (advanced method for accurate, robust, and efficient spectral fitting) [19]. In addition, constrained signal frequencies and damping factors were used in methods such as the frequency domain SVD [20], Extended Relaxation Based Estimator (E-RELAX) [21], and Metropolis Frequency-Selective (MeFres) [22]. The chemical shift relationship of certain chemical species was also used to improve algorithm accuracy and robustness in the Knowledge Based SVD (KNOB-SVD) [23] and the Knowledge Based Total Least Square (KNOB-TLS) methods [24]. Both algorithms estimated the relative chemical frequency using a fixed chemical shift between α- and γ-ATP and demonstrated an improvement in performance compared to the AMARES, HTLS, and HTLS-PK algorithms.

To date, few studies have focused on *in vivo* ^{31}P MRS conditions, in which chemical frequency changes could be caused by biophysiological and/or physical variations (e.g., pH value and Mg^{2+} concentration, and spatial B_0 variations). In this work we propose an algorithm termed Iterative Reduction of Interference Signal HSVD (IRIS-HSVD), which utilizes interference signals to optimize prior knowledge iteratively to separate baseline components and to estimate parameters for *in vivo* 3D ^{31}P MRS data that suffer from a low SNR. In 3D MRS experiments, whole brain ^{31}P MRS data may contain spectra with varying chemical shifts caused by B_0 inhomogeneity in different locations in addition to those due to biophysiological variants. Thus, an adaptive, baseline tolerant, and automatic algorithm is strongly desired. The IRIS-HSVD iteratively separates the signal subspace from noise and baseline subspaces by the QR decomposition. During each iteration, the interference signal (see below), which resulted from inaccurate prior knowledge, is identified and utilized to optimize the parameter estimation. The resulting signal frequencies and damping factors corrected by the interference signal are then used as the "new" prior knowledge for the next iteration. This procedure continues until the interference signal is minimized. This algorithm utilizes a constrained decision making mechanism and is fully automated and relatively robust.

2. Materials and methods

2.1. FID signals modeling

The complex time domain free induction decay (FID) signal is often modeled by the sum of exponentially damped sinusoids given in Eq. (1).

$$\begin{aligned} y_n &= \bar{y}_n + e_n = \sum_{k=1}^{K} c_k z_k^n + e_n \\ z_k &= e^{(-d_k + i f_k)2\pi\Delta t} \\ c_k &= a_k e^{i\phi_k} \end{aligned} \tag{1}$$

where y_n represents the original signal, $\bar{y}_n$is the estimated signal, e_n is a complex white Gaussian noise, and n is the index of data samples. The value K is the number of different frequencies and z_k refers to the k_{th} signal pole with a frequency of f_k and a damping factor of d_k (the reciprocal of the transverse relaxation time constant, T_2^*), and Δt is the data sampling time interval [8,18]. The value c_k is the complex amplitude of z_k, a_k is the absolute magnitude, and φ_k is the phase.

In this work, we develop an algorithm based on the state-space approach to solve Eq. (1). Since details of the state-space method can be found elsewhere [25], we are brief here. In short, by arranging y_n ($n = 0, \ldots, N-1$) in Eq. (1) into a special L by M Hankel matrix as shown in Eq. (2), the parameters z_k and c_k can be estimated by computing the SVD of $\mathbf{H} = \mathbf{U}\mathbf{\Sigma}\mathbf{V}^{\mathbf{H}}$, where $\mathbf{\Sigma}$ is a diagonal matrix containing the singular values, $\mathbf{U}$ and $\mathbf{V}$ is an L by L and M by M unitary matrix, respectively, and $\mathbf{H}$ denotes Hermitian conjugation [8,11].

$$\mathbf{H} = \begin{bmatrix} y_0 & y_1 & \cdots & y_{M-1} \\ y_1 & y_2 & \cdots & y_M \\ \vdots & \vdots & \vdots & \vdots \\ y_{L-1} & y_{N-M} & \cdots & y_{N-1} \end{bmatrix} \tag{2}$$
$$L \geqslant K, \quad M \geqslant K, \quad N = L + M - 1$$

2.2. Baseline distortion modeling

As mentioned above, broad line-width peaks and/or hardware imperfection can cause baseline distortion. In this work, we assume that the broad line-width signals causing baseline distortion can be represented by an assortment of fast decaying exponentially damped sinusoids and can be considered in the singular values of the HSVD solution. This is reasonable since the fast decaying part of FID is likely, in most *in vivo* ^{31}P MRS, the signal from macromolecule-bonded compounds such as cell membrane phospholipids.

2.3. Determine the number of poles

To compute the singular values is straightforward; however, it is no trivial matter to determine the number of singular values, k, to represent the estimated signal, $\bar{y}_n$, which may include broad line-width components. Several methods have been proposed to determine the number of singular values, but the decision of the number of singular values to be used can be difficult [9]. In ideal cases, we should choose a maximum number of k to represent y_n with as little noise as possible. Some investigators have recommended the use of the ratio of $\sigma_{m+1}/(\sigma_m - \sigma_{m+1})$ as a guideline for choosing the value of k [25]. The values σ_m and σ_{m+1} are the smallest accepted and the largest rejected singular value of the Hankel matrix in Eq. (2), respectively, where m (i.e., k) and $(m+1)$ are the indices of the singular values. However, in this study, we used the ratio of $\sigma_{m+1}\sigma_m/(\sigma_m - \sigma_{m+1})^2$ as the function of singular value index (m) instead of $\sigma_{m+1}/(\sigma_m - \sigma_{m+1})$. Otherwise, the decision making procedure is the same as the original method proposed by de Groen [25]. This ratio provides a compatible tool for determining the number of poles to be used and will be used through this work.

2.4. Prior knowledge and adaptive optimization processes

As noted, the HSVD method does not necessarily return the solutions (poles) with physiological and biochemical meaningful frequencies and damping factors. What it yields in most cases is a mathematically best "fit" to y_n. This drawback is particularly apparent in *in vivo* data when the SNR is significantly low. Therefore, known information such as frequencies and damping factors can be helpful for parameters optimization and fast converging in data analysis. Perhaps the most challenging task in the development of an algorithm for MRS quantitation is to have the ability of self-correction for prior knowledge when needed. It is shown that the phase change of a signal pole is strongly correlated with its frequency deviation from the original value [17]. Therefore, one may utilize phase alternation information to assist in correcting frequency mismatch if needed in the optimization process. Indeed, we found that the frequency difference of a pole from its "true" value can be approximated by the product of its phase change and its damping factor, that is, $\Delta f_k \cong \Delta p_k * d_{k0}$. We have demonstrated this relationship in Fig. 1. To assess this relationship, a set of ^{31}P MRS data was simulated by varying the frequency of certain peaks (Pi, α-, β-, and γ-ATP) using parameters listed in Table 1. Briefly, two baselines were added to the simulation data with SNR levels ranging from 100 to 1100. (see Section 2.7 for details) Note that the frequencies of Pi, α-, β-, and γ-ATP peaks varied linearly between −1

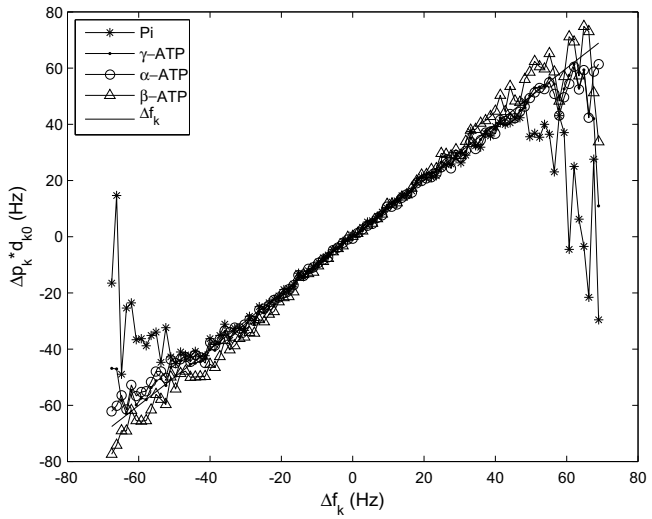

Fig. 1. The relationship between values of $\Delta p_k{*}d_{k0}$ and those of Δf_k for peaks Pi and ATPs (as indicated by symbols and lines). The value Δp_k represents a phase difference between the estimated phase value (p_{ke}) and original value (p_{k0}) of the resonances of interest after the signal was performed with the HTLS-PK. The value d_{k0} represents the original damping factor of the signal pole. The value Δf_k has a unit of Hz and so does $\Delta p_k{*}d_{k0}$. Each symbol represents a result obtained with a set of simulated data (synthesized using Table 1 parameters) using HTLS-PK. The value of Δf_k is also plotted to show the closeness of its value to those of $\Delta p_k{*}d_{k0}$.

Table 1
Parameters used for simulated spectra

Peak	f_k (ppm)	D_k (Hz)	a_k (a.u.)	φ_k (rad)
PME	6.87 ± 0.0	30	1135	0.0
Pi	4.72 ± 0.5	20	535 ± 10%	0.0
PDE	3.20 ± 0.0	30	1270	0.0
PCr	0.00 ± 0.5	12	1060	0.0
γ-ATP	−2.37 ± 0.0	22	1310 ± 10%	0.0
α-ATP	−7.48 ± 0.5	22	1310 ± 10%	0.0
β-ATP	−16.2 ± 0.5	29	1310 ± 10%	0.0
Base 1	0.05 ± 0. 0	270	3460	0.0
Base 2	4.23 ± 0.0	1140	1445	0.0

and +1 ppm from their "true values". Other resonance frequencies were invariable since these peaks are usually insensitive to biophysiological environment. Applying HTLS-PK to the simulated data, both estimated frequency (f_{ke}) and estimated phase (p_{ke}) values can be obtained for all resonances. In Fig. 1, the products of phase changes and damping factors for the Pi, α-, β-, and γ-ATP peak were plotted as a function of frequency shift. Other peaks were not shown since their frequencies were unchanged. Here, Δf_k represents the difference between f_{ke} and the "true" frequency (f_{k0}) of the signal pole of interest. The value Δp_k represents the difference between p_{ke} and the "true" value (p_{k0}). The value d_{k0} represents the true damping factor value of the simulated signal, which is assumed to be the same as the prior knowledge. It clearly demonstrates that Δf_k is strongly linearly correlated with $\Delta p_k{*}d_{k0}$ (shown in Fig. 1). The only exception is the deviation of Pi at frequency shift near ±1 ppm. The reason for this deviation is unclear at this time, but it is probably due to the influence of the nearby PME and PDE peaks. At $\Delta f_k = 0$, we also noted that the Δp_k variance (the standard deviation) increases as noise increases. An example is shown in Fig. 2, where the average absolute value of Δp_k for Pi resonance is plotted as the function of SNR. This implies that the accuracy of finding the "true" poles depends on the signal's SNR. This relationship also allows us to determine the origin of Δp_k (i.e., whether it is caused by Δf_k or signal noise). Thus, the relationship between Δp_k and SNR, which is determined by an empirical fitting, can be utilized as a convergence criterion in the optimization process (more below). In other words, if the SNR of a signal is known the convergent Δp_k value used for automatic processing is determined by the empirical equation obtained from Fig. 2. We defined this convergence criterion as the frequency phase mismatch threshold (Δp_{f0}) for a given SNR.

2.5. Fine tuning by the identification of interference signals

Imperfect frequency estimation (i.e., when $f_{ke} \neq f_{k0}$) not only caused the phase to be mismatched as described above but also resulted in non-noise type residual signals. In general, the non-noise residual spectrum $D(f)$ can be expressed in the following form:

$$D(f) = S(f_{ke}) - S(f_{k0}) = \frac{a_{ke}}{d + \mathrm{i}(f - f_{ke})} - \frac{a_{k0}}{d + \mathrm{i}(f - f_{k0})} \quad (3)$$

where $S(f_{k0})$ and $S(f_{ke})$ are the spectra of the "true" and estimated signals with frequencies of f_{k0} and f_{ke}, respectively; and a_{k0} and a_{ke} are their amplitudes and d is the common damping factor for both signals. The real part of this equation is a differentiated Lorentzian function [27]. Here, we assume that the damping factor does not contribute significantly in the $D(f)$, which is found to be true in most cases.

Fig. 3 illustrates this concept using the $D(f)$ of the α-ATP peak as an example. The spectra from top to bottom of each panel represent $S(f_{k\ 0})$, $S(f_{ke})$, and $D(f)$, respectively. These estimated results, $S(f_{ke})$, were obtained using the non-iterative HTLS-PK method, thus the results heavily depend on prior knowledge. Fig. 3a, where $f_{ke} = f_{k0}$, shows a typical white Gaussian noise type of residual sig-

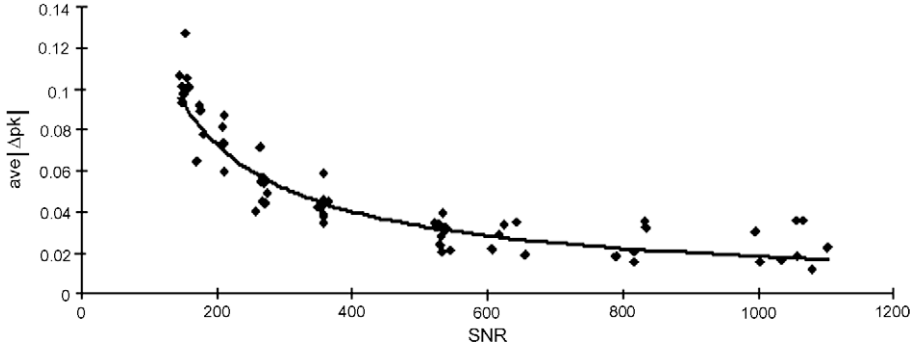

Fig. 2. An example of the frequency phase mismatch threshold. The average absolute value of Δp_k for Pi resonance at $\Delta f_k = 0$ is plotted as the function of SNR, which can be represented by an exponential line. Each symbol was an average result arising from 200 Monte Carlo simulation studies with a given condition using HTLS-PK. For this particular example, an empirical equation ($y = 7.0x^{-0.86}$) is found and indicated by a solid line. Here, x represents the SNR value of the signal and y the frequency phase mismatch threshold (Δp_{f0}).

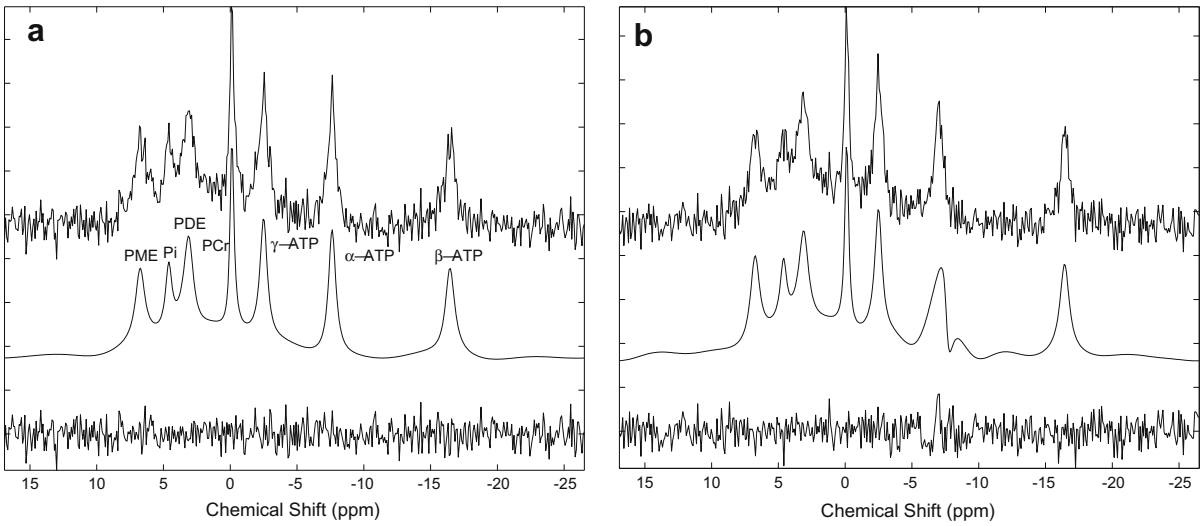

Fig. 3. Demonstrations of Interference signal using HTLS-PK with simulated data. (a) A condition that all of the estimated frequencies match the true values and the residual signals are primarily white Gaussian noise. On the contrary, (b) shows conditions where the estimated frequency of the α-ATP peak is 0.23 ppm smaller than the true values. Consequently, non-white-noise signals are revealed in these residual signals, which are termed the interference signals (see text for details). Each figure exhibits, from top to bottom, the original, the estimated and the residual signals, respectively.

nal, while Fig. 3b, where $f_{ke} \neq f_{k0}$, exhibits both noise and non-noise type residual signals. The prior knowledge of α-ATP frequency was intentionally shifted to 0.23 ppm up-field (Fig. 3b). The result (data not shown) with 0.23 ppm down-field shifting was similar to Fig. 3b. We termed the non-noise residual signals "interference signals", whose "interference poles" can be identified from the residual signal by the HSVD method. It was observed that a larger Δf_k can result in an identifiable interference pole and phase change ($\Delta p_k > 3\Delta p_{f0}$) while a smaller Δf_k can only introduce a visible phase change ($\Delta p_{f0} < \Delta p_k < 3\Delta p_{f0}$). Therefore, the interference poles can fine tune prior knowledge in the adaptive optimization process. Specifically, the interference signals can be added or "compensated" into the estimated signals where the non-noise residual signals were found. After quantifying the "compensated" estimated signals with HSVD, the resulting poles are then assigned to "new" prior knowledge poles for the next iteration. The fine tuning process will be repeated until no interference signals (i.e., when $\Delta p_k < 3\Delta p_{f0}$) can be identified. We also did similar simulation studies for the effects of damping factors and found that even if the prior knowledge damping factor d_{ke} varied by a range of ±20% of d_{k0} values, no non-noise residual signals were observable. This suggests that non-noise residual signals may not be able to assist in the fine tuning of the damping factors.

2.6. Summary of IRIS-HSVD

The IRIS-HSVD algorithm is summarized in the following five steps.

1. Acquiring prior knowledge: All prior knowledge should be determined and initiated at the beginning. Details for setting up prior knowledge for simulation and *in vivo* data are given in Sections 2.7 and 2.9, respectively.
2. Acquiring p estimated poles, z_e: Supposing there are p resonances of interest (p is the prior knowledge and decided by the investigators), the number of total signal poles k ($k > p$) are determined by the HSVD method described in Section 2.3. Then use the HTLS-PK according to the approach reported by Chen et al. [17] to separate the signal of interest from the background noise and baseline signal. Specifically, based on the prior knowledge, the QR decomposition is used to estimate the poles of interest (z_e). Then, the residual signal (containing noise and non-noise residuals) is separated by removing z_e from the original signal. The result is composed of two parts: the estimated compounds' signal of interest (y_e) with a complex amplitude (c_e) and the residual signal (y_r).
3. Identification and quantification of interference signals: The phase of $c_e(p_{ke})$ is compared to the known (original or prior knowledge) phase ($pk0$) to determine the difference (Δp_k), which is compared to Δp_{f0} (described in Section 2.4) along with the SNR. Interference signal poles are identified at the peaks with "large" phase changes (i.e., $\Delta p_k > 3\Delta p_{f0}$) by the HSVD method. The interference signal is reconstructed from these poles.
4. Prior knowledge poles correction: The interference signal is added to the estimated compounds' signal of interest (y_e) to approximate the true compounds' signal. Then, the HSVD is used to estimate the "true" compounds' poles, which is set to be the new prior knowledge for the next iteration if it does not meet the convergence criterion (see Step 4). For poles with a "small" phase change (i.e., $\Delta p_{f0} < \Delta p_k < 3\Delta p_{f0}$), the relationship of $\Delta f_k \cong \Delta p_k * d_{k0}$ is used to estimate the true frequency. The new prior knowledge poles are composed accordingly with the same damping factors. Since Δp_{f0} for *in vivo* situation is difficult to obtain, the simulated results from Fig. 2 were applied to all data in this work.
5. Iterative optimization of interference signal: Repeat steps 2–4 with updated prior knowledge poles until the interference signal becomes negligible (i.e., $\Delta p_k < \Delta p_{f0}$).In our case, a maximum of 6 iterations was set to prevent oscillation and it seems to work reasonably well for our case and only about less than 20% of *in vivo* data reach the maximum number of iterations due to low SNR. The convergence time for a typical 2.4 GHz dual processor PC is about 3 to 6 s depending on SNR.

2.7. Simulation data

All simulation data for ^{31}P MRS was synthesized using Eq. (1) and parameters listed in Table 1. These parameters were obtained from data published in the literature [26] and our own work. Two broad line-width peaks were added to the simulated ^{31}P spectra, which were determined by our observation of human brain ^{31}P

data at 4T. Presumably, these broad component signals originated from immobile membrane phospholipids metabolites [28] and/or hardware imperfections. The two broad peaks were located at 0.05 and 4.23 ppm (reference to PCr) with a line-width of about 270 and 1140 Hz, respectively. These synthesized data were used for all Monte Carlo studies. To mimic *in vivo* data signals, white Gaussian noises with various standard deviations were added. We defined the SNR ratio in the following equation:

$$\mathrm{SNR} = \frac{\sqrt{\sum_{k=1}^{p} a_k^2}}{\sigma} \tag{4}$$

where σ; is the standard deviation of the noise. For both simulated and measured *in vivo* data, the last 20% of the data points in each FID were defined as noise. A medium range of noise standard deviation for simulated data was chosen to approximate the SNR ratio of the *in vivo* data after commonly used digital filtering (e.g., exponential and Gaussian filters) was applied to the data [29]. This common practice of applying digital filtering improves the SNR; hence, the choice of a medium SNR range seems to be more useful than that in the extreme cases with heavy noise levels.

Considering *in vivo* biochemical conditions, the chemical frequency values of Pi, α-ATP, β-ATP, and γ-ATP of the simulation data are allowed a variance of ±0.5 ppm. Their amplitudes and damping factors also allowed a total of 10% change from their original values. The levels of baseline distortion and noise were comparable or even higher than the human *in vivo* data obtained from our laboratory. These data were used to test the performance of IRIS-HSVD and compared to the results with those using HTLS-PK and HSVD algorithms. Note that the prior knowledge is the data from the "true values" of the Table 1 and is used for all algorithms.

2.8. Performance evaluation for simulation data

The performance of three methods was evaluated by the relative root mean squared error (RRMSE), defined in Eq. (5), for all chemical compounds.

$$\mathrm{RRMSE}_k = 100\sqrt{\frac{1}{\Upsilon}\sum_{\upsilon=1}^{\Upsilon}\frac{\left(\zeta_k - \hat{\zeta}_k^{\upsilon}\right)^2}{\zeta_k^2}} \tag{5}$$

where γ is the number of Monte Carlo trials for each given parameter set. We chose 200 in our test. The value ζ_k denotes one of the k_{th} targeted compound parameters (i.e., ω, d, c, or φ) as described in Eq. (1), and $\hat{\zeta}_k^{\upsilon}$ is the estimated value from one of the above algorithms obtained in the υth trial.

The Cramer–Rao lower bounds (CRB), the lowest possible error in an ideal estimation, were also included to demonstrate the performance of the proposed method [30,31]. The CRBs for frequency, damping factor, amplitude and phase are expressed as follows:

$$\mathrm{CRB}_f = \mathrm{CRB}_d = 2\sqrt{2}(-d)^{3/2}\sqrt{\Delta t}\frac{\sigma}{c} \tag{6}$$

$$\mathrm{CRB}_c = c\mathrm{CRB}_\phi = 2(-d)^{1/2}\sqrt{\Delta t}\sigma \tag{7}$$

The symbols f, d, c, φ, σ, and Δt were defined previously. Note that the CRB values estimated here assumed that all peaks are independent (i.e., single peaks); therefore, the values are at best a first approximation for conditions with multiple peaks. Consequently, the calculated CRB values are too small to represent a multiple peaks' condition due to correlation effects in our cases, which are evident from our results shown in Fig. 4 (see below).

2.9. In vivo brain MRS data quantification

All *in vivo* MRS data were collected at the Center for Imaging Research at the University of Cincinnati using a 4.0 T Varian Unity INOVA whole body MRI/MRS system (Varian Inc., Palo Alto, CA). 3D ^{31}P MRS data were acquired with a ^{1}H/^{31}P double-tuned TEM coil using a 3D one-pulse sequence. A 3D phase encoding scheme was used with acquisition weighting according to a Gaussian function to minimize side lobe ripple while retaining optimal signal-to-noise [32]. The ^{31}P MRS data were acquired with a 3 s TR, 928 phase encoding steps, 90° flip angle and 1 average. The B_1 excitation bandwidth covers about 5 KHz, which was experimentally verified. Total acquisition time was about 45 min. Single voxel MRS data were obtained by using an image guided single voxel reconstruction method in the specified region of interests based on a 3D MDEFT image [33] acquired from the same subject. The advantage of using a one-pulse sequence for data acquisition is to get a better SNR since the signal is detected with a very short delay time. However, the disadvantage lies in the baseline distortion caused by the inclusion of signals from immobile membrane phospholipids metabolites. All data were applied with a 15 Hz exponential apodization before further processing.

First, prior knowledge (i.e., f_{ke} and d_{ke}) of the ^{31}P resonances of interest was obtained from the average spectrum of the entire 3D MRS data set, which is equivalent to the signal from the center of k-space. Using HSVD, it was relatively easy to estimate the chemical frequencies and damping factors of the metabolites of interest because of its good SNR. However, the d_{ke} values might be larger compared to those in the local MRS due to B_0 inhomogeneity since the signal was averaged from the entire volume. These slightly larger damping factors do not affect the performance of the IRIS-HSVD, since it is insensitive to moderately imperfect damping factors. After acquiring prior knowledge, data were preprocessed with an exponential filter before performing the IRIS-HSVD algorithm as described previously.

The PCr peak was easily identified and quantified by the HSVD because of its relatively stable chemical shift. After that, the estimated PCr resonance frequency and phase were used as reference values to correct for frequency shifts and the zero order phases of other resonances. The ratio of the estimated PCr damping factor to the prior knowledge value was used to modify d_{ke} for other chemical compounds of interest to adjust for local damping factor change caused by B_0 variation.

The same prior knowledge and same data sets with their two initial data points removed were also processed with AMARES for comparison. All AMARES quantifications were performed using the jMRUI package without modification with the begin time fixed and the zero order phase variable. Note that we also tried various parameter settings and found the above mentioned setting yielding the most valid result.

3. Results and discussion

3.1. Quantitation of simulated NMR signals

Fig. 4 showed CRBs of frequency and amplitude for Pi, γ-ATP and α-ATP peaks, and their corresponding RRMSEs resulting from the HSVD, HTLS-PK, and IRIS-HSVD methods. The CRB and RRMSEs are plotted as a function of the noise standard deviation. Fig. 4a, c, and e depicts the accuracy of frequency estimation in different noise levels for Pi, γ-ATP and α-ATP peaks using three different methods, while Fig. 4.2b, d, and f illustrates the accuracy of the amplitude estimation. In general, the frequency estimations have smaller RRMSE values and are more reliable than that of amplitude. HSVD performs better in the frequency estimations than in the amplitude estimations as compared to HTLS-PK in the noise level tested. In this study, the prior knowledge frequency was fixed but the estimated frequencies varied in Monte Carlo simulations. Thus, there is no surprise that HTLS-PK performed poorly as compared to HSVD since HTLS-PK, but not HSVD, relies heavily on the

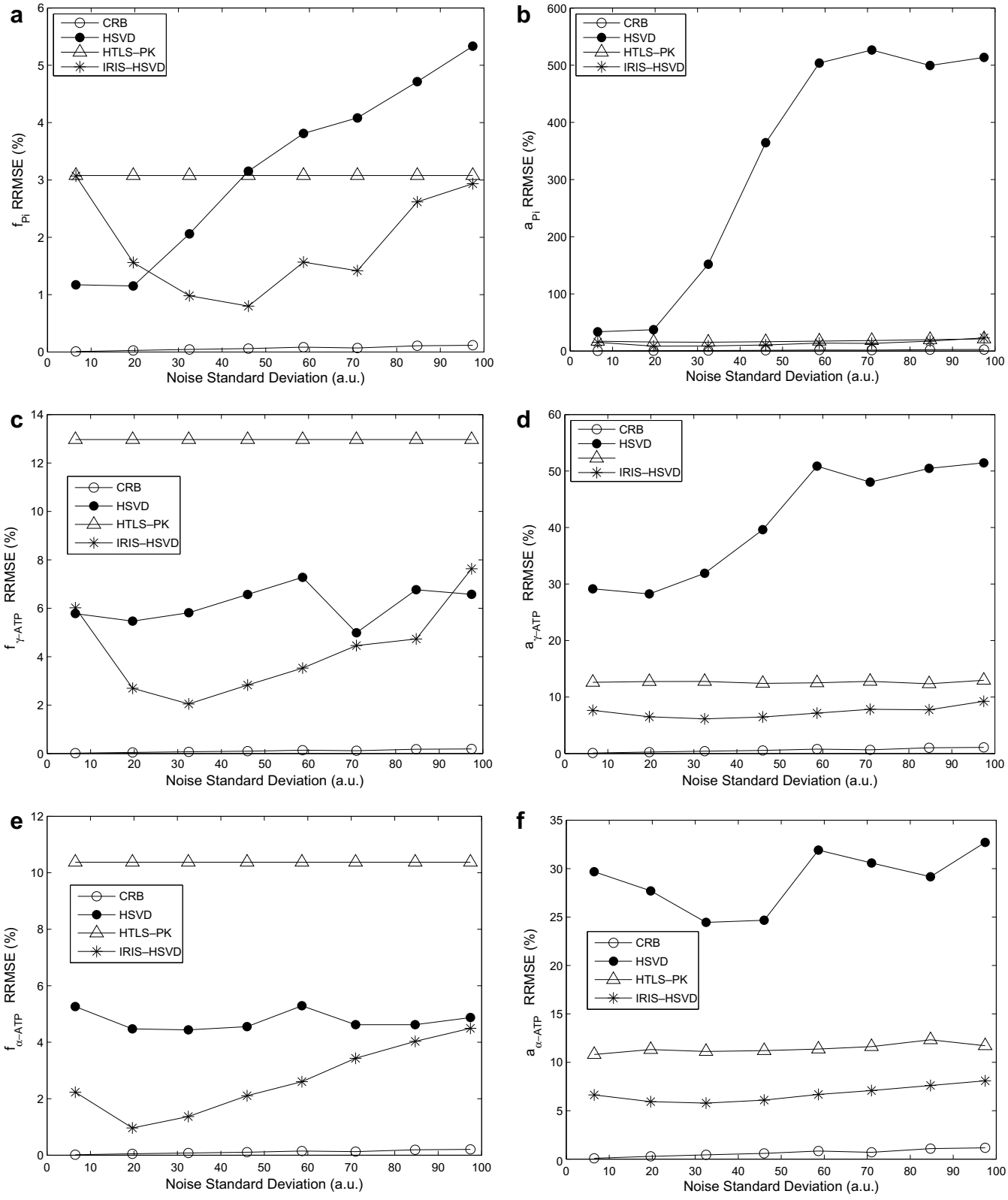

Fig. 4. Performance evaluation for IRIS-HSVD, HTLS-PK, and HSVD using Monte Carlo studies. Symbols represent the simulation result in given conditions (see text for details), while lines are only to guide eyes. Peaks Pi (a and b), γ-ATP (c and d), and α-ATP (e and f) are given for demonstration. The values estimated for CRB and RRMSE of frequency (a, c, and e) and amplitude (b, d, and f) are shown for all three methods.

accuracy of the prior knowledge. Note that the frequency RRMSE values resulting from the HTLS-PK were independent of noise levels since the prior knowledge frequency value is identical to the mean value of the estimated frequencies (i.e., $\xi_k = \frac{1}{\gamma}\sum_{\nu=1}^{\gamma}\xi_k^{\nu}$) in Monte Carlo simulations. If one considers 10% RRMSE as the highest limit for achieving a reliable quantification result, all three tested methods performed relatively well for the frequency estimation but only IRIS-HSVD performed satisfactorily for both fre-

quency and amplitude. Furthermore, IRIS-HSVD outperformed the other two methods in all aspects.

In general, the results show RRMSE and CRB values increase as noise increases. This is reasonable since adding noise increases the uncertainty of the Monte Carlo experiments resulting in an increased RRMSE. However, it was surprising that the performance of IRIS-HSVD seemed poor for the frequency estimation in very low noise ranges. It is possible that the better SNR signals resulted in oversensitivity in the identification and quantification of interference signals (see Section 2.6), which jeopardized the accuracy of performance. Nevertheless, this drawback does not significantly impede its ability to find the right frequency, and particularly the amplitude.

3.2. Quantification of in vivo ^{31}P MRS signal

Fig. 5 shows the result of a typical *in vivo* ^{31}P MRS spectrum. The top panel shows the residual signal and the second panel shows the estimated peaks of the seven ^{31}P compounds of interest individually. The third panel illustrates the estimated spectrum overlaid with the original signal, demonstrating the estimation accuracy. The bottom panel shows the original spectrum together with the estimated baseline, which demonstrates IRIS-HSVD successfully separating the distorted baseline from the signal of interest. The estimated results are shown in Table 2 along with the prior knowledge values used for the IRIS-HSVD algorithm. The table shows chemical shift frequencies and damping factors for all resonance peaks. The result showed that all prior knowledge frequencies, except for the Pi peak, are identical to the final estimated frequencies resulting from IRIS-HSVD. In addition, all prior knowledge damping factors agreed very well with the final estimations. This suggests that the spectrum from the *k*-space center of the 3D data, which is equivalent to an average spectrum of the entire volume of interest, is an excellent prior knowledge for MRS data processing. The observation of a 0.11 ppm chemical shift for the Pi peak most likely reflects a variation of local pH level and/or Mg^{2+} concentration of brain tissues.

Table 2
The prior knowledge values and estimated results using IRIS-HSVD for a typical *in vivo* spectrum shown in Fig. 5

Peak	Prior knowledge		Final estimated results	
	Frequency (ppm)	Damping factor (Hz)	Frequency (ppm)	Damping factor (Hz)
PME	6.87	32	6.87	35
Pi	4.86	18	4.75	20
PDE	2.78	38	2.78	41
PCr	0.00	12	0.00	13
γ-ATP	−2.53	20	−2.53	22
α-ATP	−7.55	20	−7.55	22
β-ATP	−16.4	25	−16.4	27

The AMARES method in the jMRUI package [34,35], a currently available ^{31}P MRS data processing software, was chosen for comparison to the performance of IRIS-HSVD. AMARES could quantify the raw signal used in Fig. 5 if the baseline signal prior knowledge is available, but such information can be difficult to acquire. Therefore, the first 2 points of the original signal were removed to minimize baseline distortion and the phase was adjusted correspondingly before data were submitted to IRIS-HSVD and AMARES for quantification. Figs. 6 and 7 show the quantified spectrum obtained from IRIS-HSVD and AMARES methods, respectively. Note that Fig. 7 was the output directly from the jMRUI package without further modification. The panels, from the top to the bottom, exhibit the residual signals, individual resonance components, the estimated spectrum, and the original spectrum, respectively. Both methods successfully identified all targeted resonances. Unlike AMARES, IRIS-HSVD not only classifies the chemical compounds of interest but also the distorted baseline. This is not surprising since AMARES precludes a distorted baseline. Therefore, the result from the IRIS-HSVD may provide a better estimated spectrum than AMARES. This can also be illustrated by the fact that the residual signal standard deviation (SD) is about 40% more in Fig. 6 (SD = 3247 a.u.) as compared to Fig. 7 (SD = 4784 a.u.). Furthermore, the residual signal in Fig. 6 resulting from IRIS-HSVD

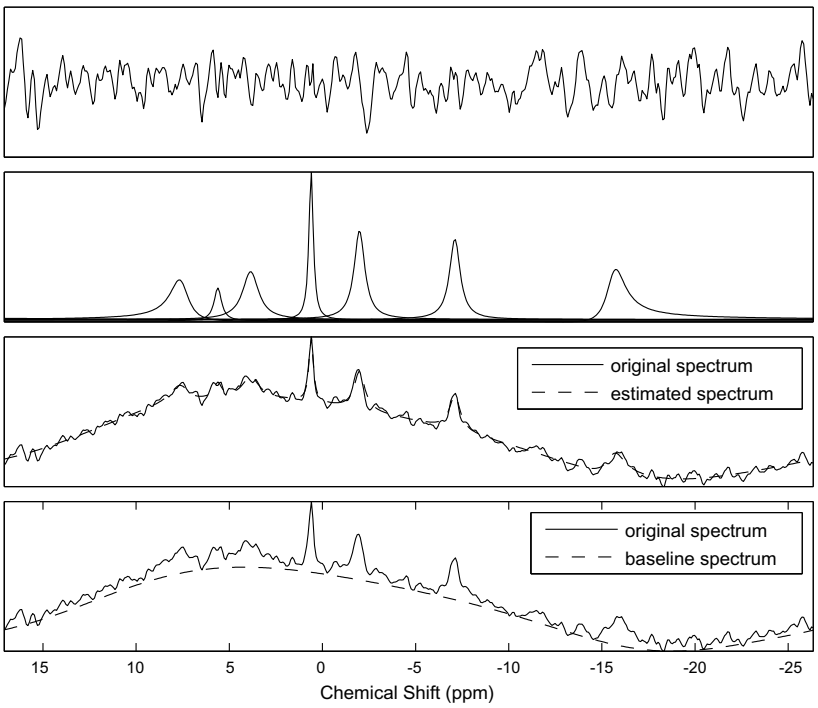

Fig. 5. A typical result of *in vivo* (raw) data analyzed by IRIS-HSVD. It shows from the top to the bottom the residual signal, the individual estimated spectrum for major chemical compounds of interest, the original spectrum overlaid with the estimated spectrum, and the original spectrum along with an estimated baseline.

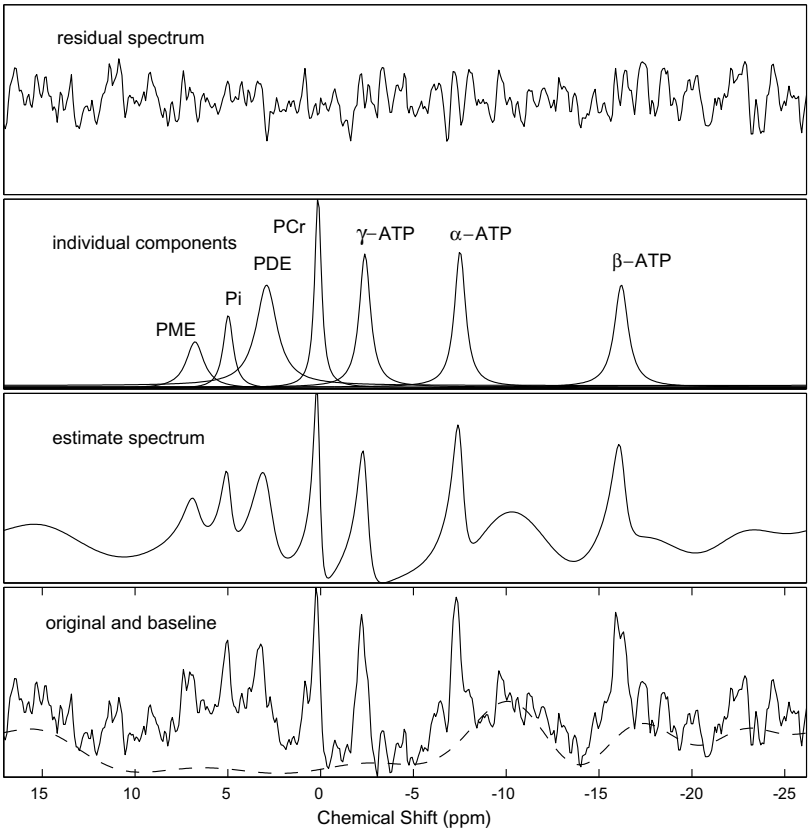

Fig. 6. A typical example of truncated *in vivo* data analyzed by IRIS-HSVD. This figure demonstrates the quantification of the same spectrum shown in Fig. 5 but with the first 2 time domain points removed. The figure shows, from the top to the bottom, the residual signal, the individual estimated spectrum, the estimated spectrum, and the original spectrum along with an overlaid estimated baseline.

contains mainly white Gaussian noise, while that in Fig. 7 includes some features in addition to the white Gaussian noise signal. We showed the numerical results from both methods in Table 3. Because of the influence of the distorted baseline, the estimated amplitudes between these two methods may not be comparable. In general, the resulting frequencies were quite similar between these two methods, while estimated damping factors were larger in those obtained by IRIS-HSVD. Due to the significant difference in damping factors, the amplitudes estimated by these two methods, the most important components in MRS data analysis, were quite different. While there are no grounds to verify which method is more accurate in amplitude estimation, one would probably agree that IRIS-HSVD may perform better if judged by some biophysiological guidelines. For example, the estimated amplitudes of α-, β-, and γ-ATP were quite similar for the IRIS-HSVD method, but they varied significantly when using the AMARES approach. One would expect that these amplitudes to be identical if B_1 is strong enough, since each signal represents one phosphorus nucleus from the same compounds but with a different chemical environment.

In order to compare the performance of these two methods, we sampled about 40 spectra from different locations in the brain from one subject. After 15 Hz exponential filtering, untruncated data were quantified by IRIS-HSVD with the prior knowledge as described previously. For AMARES quantification, data were truncated for the first 2 time domain data points before data analysis using the same prior knowledge. A semiautomatic HSVD method, which involved operator interaction, was used to determine the "true values" of all frequencies and damping factors for our performance comparison. However, the comparison for amplitude and phase between these two methods may not be practical because of a different data size used between the IRIS-HSVD and AMARES methods. Therefore, only frequencies and damping factors resulting from these two methods were compared to the "true" values, which were presented in Table 4 for seven major ^{31}P resonances in the brain. Again, the results from both methods are generally quite compatible and there is no significant difference between them. However, one should note that IRIS-HSVD analyzes the raw data and AMARES processes the truncated data. It is noted that similar results were observed when truncated data were processed by IRIS-HSVD (data not shown). It should also be noted that both AMARES and IRIS-HSVD performed relatively well in resonances that have a relatively high SNR (e.g., ATPs and PCr). Nevertheless, IRIS-HSVD showed a slightly smaller mean and standard deviation in frequency for PDE and Pi peaks as compared to AMARES. Generally, IRIS-HSVD demonstrates better performance in the damping factor estimation, which may result in a more stable presentation in amplitude estimation as compared to AMARES. A better performance for IRIS-HSVD may be attributed to its ability to compensate for the distorted baseline problem in Pi-PDE region, which results in a more robust estimation.

4. Conclusion

We have demonstrated with simulated and *in vivo* data that the performance of IRIS-HSVD is superior to the performance of HTLS-PK and HSVD. The major advantage of IRIS-HSVD is its ability to process any raw data, particularly for those suffering from baseline distortion. This ability not only increases data quantification consistency but also theoretically improves estimation accuracy. Furthermore, no interactive phase correction or data preprocessing, other than an exponential filter, are required. These features make IRIS-HSVD a viable candidate for large volume MRS data processing and a truly automatic algorithm.

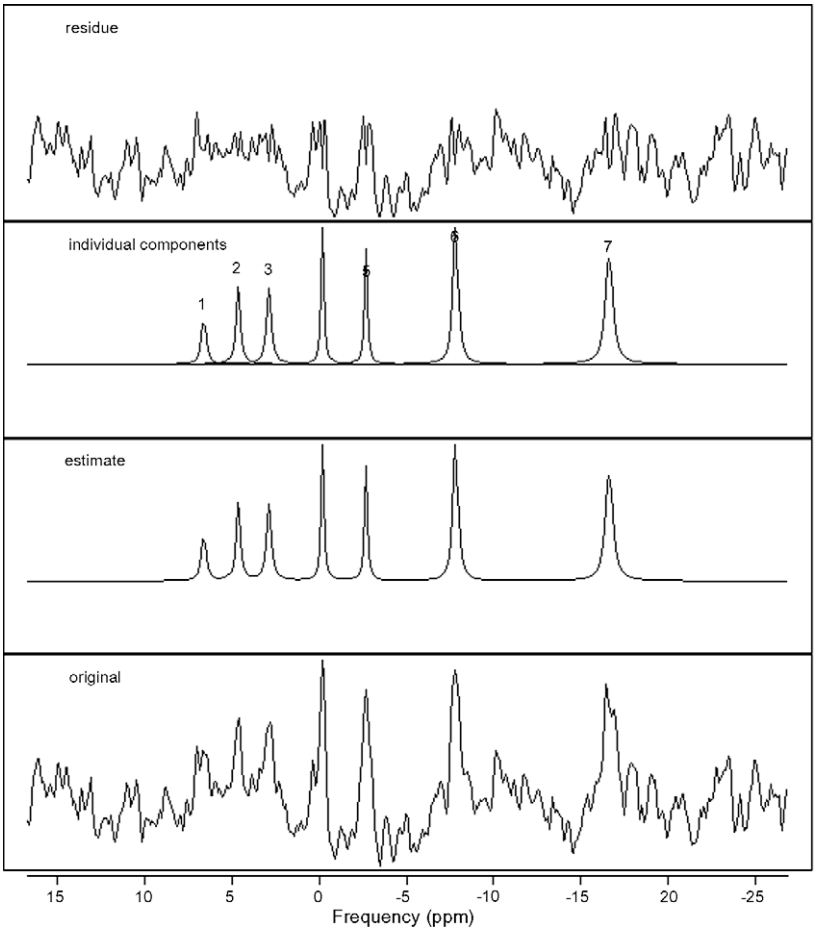

Fig. 7. A typical example of truncated *in vivo* data analyzed by AMARES. This figure demonstrates the quantification of the same data shown in Fig. 6. A zero order and a first order phase correction were performed using tools in jMRUI before analysis by AMARES. The prior knowledge used in Figs. 5–7 were identical. The graphic output was adapted from jMRUI software package without modification. The figure shows from the top to the bottom the residual signal, the individual estimated spectrum, the estimated spectrum, and the original spectrum.

Table 3
Comparison quantification results for a typical *in vivo* spectrum between IRIS-HSVD (Fig. 6) and AMARES (Fig. 7)

Peak	IRIS-HSVD				AMARES			
	f_k (PPM)	d_k (Hz)	a_k (a.u.)	ϕ_k (rad)	f_k (PPM)	d_k (Hz)	a_k (a.u.)	ϕ_k (rad)
PME	6.87	40	796	0.32	6.80	11	189	2.9
Pi	4.85	22	684	0.20	4.96	10	327	2.9
PDE	2.78	47	2101	−0.10	3.07	12	373	2.9
PCr	0.00	15	1307	−0.03	0.00	6.4	401	2.9
γ-ATP	−2.53	25	1461	0.11	−2.46	7.0	341	2.9
α-ATP	−7.55	25	1557	0.39	−7.58	11	650	2.9
β-ATP	−16.5	31	1395	−0.09	−16.4	17	740	2.9

Table 4
Differences (mean ± standard deviation) in frequency and damping factor between the "true" value and the estimation values obtained by IRIS-HSVD and AMARES

Peak	IRIS-HSVD		AMARES	
	f_k (Hz)	d_k (Hz)	f_k (Hz)	d_k (Hz)
PME	14 ± 11	9.6 ± 9.2	14 ± 13	12 ± 6.6
Pi	18 ± 23	6.0 ± 5.3	21 ± 37	15 ± 10
PDE	24 ± 18	12 ± 11	51 ± 81	34 ± 44
PCr	2.1 ± 4.1	1.3 ± 1.6	8.0 ± 14	5.9 ± 2.7
γ-ATP	7.0 ± 6.4	6.4 ± 5.5	9.0 ± 6.7	14 ± 5.6
α-ATP	8.1 ± 9.0	5.8 ± 4.9	4.7 ± 4.5	8.8 ± 5.6
β-ATP	15 ± 15	6.6 ± 5.0	10 ± 10	14 ± 6.4

IRIS-HSVD, similar to HSVD, assumes that the signal to be processed comprises a pure Lorentzian lineshape. This may raise a concern for *in vivo* MRS data since some researchers suggested that such data is best represented by a Gauss or Voigt model [36]. However, our results show that IRIS-HSVD performs well with both simulation and *in vivo* data. These results, which seem to agree with others that used HSVD based methods [4–6], suggest that IRIS-HSVD may not be sensitive to lineshape models or that the *in vivo* MRS signals are quite close to a Lorentzian lineshape. Furthermore, the fact that IRIS-HSVD treats all peaks as singular may be too simplistic. For example, the resonance for γ-ATP and α-ATP should be doublet and β-ATP triplet. However, since ^{31}P resonances at 4 T usually appear as singlet, this simplified model may be sufficient which is supported by our results.

Like other algorithm, IRIS-HSVD has its weaknesses. The current version of IRIS-HSVD requires restricting the iteration number to avoid unwanted oscillation. Also, poor performance of simulated results in Fig. 4 at the low noise region is unexpected, which may be attributed to imperfect convergence criteria chosen in the process. These could include criteria for the determination of the pole number and/or the frequency phase mismatch threshold. Besides, fine tuning for the damping factors was neglected, which may affect the accuracy of amplitude estimation. Optimizing those criteria and considering a complete model (i.e., using multiplets instead of singlet) may further improve the performance of IRIS-HSVD and is worthwhile further exploration. In addition, since this method is verified only for ^{31}P signals at 4 T, it needs further test-

ing to determine if this algorithm will also work for other types of signals (^{1}H, ^{13}C, etc.) or signals from different field strengths in the future.

Perhaps the novel contribution of IRIS-HSVD, as compared to other similar algorithms, is the use of a constrained recursive approach, which continues to modify the prior knowledge so that a "targeted" value may be reached after a few iterations. Therefore, careful selection of the prior knowledge is important as this will determine the convergence speed for the process. From our study, the spectrum from the *k*-space center proved to be an excellent initial starting value for 3D spectroscopic data.

Acknowledgments

The authors thank Dr. Wen-Jang Chu and Mr. Judd Storrs for their thoughtful discussions. We would also like to thank Drs. William Ball and Stephen Strakowski for their generous support of this study, and Ms. Kati Elfers for her proofreading of this manuscript.

References

[1] J.S. Cohen, J.W. Jaroszewski, O. Kaplan, J. Ruiz-Cabello, S.W. Collier, A history of biological applications of NMR spectroscopy, Prog. Nucl. Magn. Spectrosc. 28 (1995) 53–85.
[2] I.C.P. Smith, L.C. Stewart, Magnetic resonance spectroscopy in medicine: clinical impact, Prog. Nucl. Magn. Spectrosc. 40 (2002) 1–34.
[3] S.Y. Kung, K.S. Arun, D.V. Bhaskar Rao, State-space and SVD-based approximation methods for the harmonic retrieval problem, J. Opt. Soc. Amer. 73 (1983) 1799–1811.
[4] G.H. Golub, C. Reinsch, Singular value decomposition and least squares solutions, Numer. Math. 14 (1970) 403–420.
[5] D. Bau III, L.N. Trefethen, "Numerical Linear Algebra", Society for Industrial and Applied Mathematics, Philadelphia, PA, 1997.
[6] G.H. Golub, C.F. Van Loan, Matrix Computations, third ed., Johns-Hopkins University Press, Baltimore, MD, 1996.
[7] S. Mierisova, M. Ala-Korpela, MR spectroscopy quantitation: a review of frequency domain methods, NMR Biomed. 14 (2001) 247–259.
[8] L. Vanhamme, T. Sundin, P. van Hecke, S. van Huffel, MR spectroscopy quantitation: a review of time-domain methods, NMR Biomed. 14 (2001) 233–246.
[9] R. de Beer, D. van Ormondt, Analysis of NMR data using time domain fitting procedures, NMR Basic Princ. Prog. 26 (1992) 201–248.
[10] W.W.F. Pijnappel, A. Van Den Boogaart, R. De Beer, D. van Ormondt, SVD-based quantification of magnetic resonance signals, J. Magn. Reson. 97 (1992) 122–134.
[11] H. Barkhuijsen, R. de Beer, D. van Ormondt, Improved algorithm for noniterative time-domain model fitting to exponentially damped magnetic resonance signals, J. Magn. Reson. 73 (1987) 33–37.
[12] T. Laudadio, N. Mastronardi, L. Vanhamme, P. Van Hecke, S. Van Huffel, Improved Lanczos algorithms for blackbox MRS data quantitation, J. Magn. Reson. 157 (2002) 292–297.
[13] H. Barkhuijsen, R. de Beer, W.M.M.J. Bovee, D. van Ormondt, Retrieval of frequencies amplitudes damping factors and phases from time-domain signals using a linear least-squares procedure, J. Magn. Reson. 61 (1985) 465–481.
[14] H. Barkhuijsen, R. de Beer, D. van Ormondt, Aspects of the computational efficiency of LPSVD, J. Magn. Reson. 64 (1985) 343–346.
[15] S. van Huffel, H. Chen, C. Decanniere, P. van Hecke, Algorithm for time-domain NMR data fitting based on total least squares, J. Magn. Reson. Ser. A 110 (1994) 228–237.
[16] H. Ratiney, Y. Coenradie, S. Cavassila, D. van Ormondt, D. Graveron-Demilly, Time-domain quantitation of ^{1}H short echo-time signals: background accommodation, Magn. Reson Mater. Phys. 16 (2004) 284–296.
[17] H. Chen, S. van Huffel, D. van Ormondt, R. de Beer, Parameter estimation with prior knowledge of known signal poles for the quantification of NMR spectroscopy data in the time domain, J. Magn. Reson. Ser. A 119 (1996) 225–234.
[18] H. Chen, S. van Huffel, J. Vandewalle, Improved methods for exponential parameter estimation in the presence of known poles and noise, IEEE Trans. Sig. Proc. 45 (1997) 1390–1393.
[19] L. Vanhamme, A. van den Boogaart, S. van Huffel, Improved method for accurate and efficient quantification of MRS data with use of prior knowledge, J. Magn. Reson. 129 (1997) 35–43.
[20] P. Stoica, N. Sandgren, Y. Selen, L. Vanhamme, S. Van Huffel, Frequency-domain method based on the singular value decomposition for frequency-selective NMR spectroscopy, J. Magn. Reson. 165 (2003) 80–88.
[21] Z.Q. Bi, A.P. Bruner, J. Li, K.N. Scott, Z.S. Liu, C.B. Stopka, H.W. Kim, D.C. Wilson, Spectral fitting of NMR spectra using an alternating optimization method with *a priori* knowledge, J. Magn. Reson. 140 (1999) 108–119.
[22] R. Romano, A. Motta, S. Camassa, C. Pagano, M.T. Santini, P.L. Indovina, A new time-domain frequency-selective quantification algorithm, J. Magn. Reson. 155 (2002) 226–235.
[23] P. Stoica, Y. Selen, N. Sandgren, S. van Huffel, Using prior knowledge in SVD-based parameter estimation for magnetic resonance spectroscopy—the ATP example, IEEE Trans. Biomed. Eng. 51 (2004) 1568–1578.
[24] T. Laudadio, Y. Selen, L. Vanhamme, P. Stoica, P. van Hecke, S. van Huffel, Subspace-based MRS data quantitation of multiplets using prior knowledge, J. Magn. Reson. 208 (2004) 53–65.
[25] P. de Groen, The fit of a sum of exponentials to noisy data, J. Comp. Appl. Math. 20 (1987) 125–137.
[26] R.A. de Graaf, In Vivo NMR Spectroscopy, Principles and Techniques, John Wiley & Sons, Ltd, West Sussex, England, 1998. pp. 63–64.
[27] W. Gough, The graphical analysis of a Lorentzian function and a differentiated Lorentzian function, J. Phys. A. Ser. 2 1 (1968) 704–709.
[28] J.A. Stanley, J.W. Pettegrew, Postprocessing method to segregate and quantify the broad components underlying the phosphodiester spectral region of *in vivo* ^{31}P brain spectra, Magn. Reson. Med. 45 (2001) 390–396.
[29] H. in 't Zandt, M. van der Graaf, A. Heerschap, Common processing of in vivo MR spectra, NMR Biomed. 14 (2001) 224–232.
[30] S. Cavassila, S. Deval, C. Huegen, D. van Ormondt, D. Graveron-Demilly, Cramer-Rao bound expressions for parametric estimation of overlapping peaks: influence of prior knowledge, J. Magn. Reson. 143 (2000) 311–320.
[31] S. Cavassila, S. Deval, C. Huegen, D. van Ormondt, D. Graveron-Demilly, Cramer-Rao bounds: an evaluation tool for quantitation, NMR Biomed. 14 (2001) 278–283.
[32] H.P. Hetherington, D.D. Spencer, J.T. Vaughan, J.W. Pan, Quantitative ^{31}P spectroscopic imaging of human brain at 4 Tesla: assessment of gray and white matter differences of phosphocreatine and ATP, Magn. Reson. Med. 45 (2001) 46–52.
[33] J.-H. Lee, M. Garwood, R. Menon, G. Adriany, P. Andersen, C. Truwit, K. Ugurbil, High contrast and fast three-dimensional magnetic resonance imaging at high field, Magn. Reson. Med. 12 (1995) 308–312.
[34] A. Naressi, C. Couturier, J.M. Devos, M. Janssen, C. Mangeat, R. de Beer, D. Graveron-Demilly, Java-based graphical user interface for the MRUI quantitation package, Magn. Reson. Mater. Phys. 12 (2001) 141–152.
[35] A. Naressi, C. Couturier, I. Gastang, R. de Beer, D. Graveron-Demilly, Java-based graphical user interface for MRUI a software package for quantitation of *in vivo* Medical Magnetic Resonance Spectroscopy Signals, Comput. Biol. Med. 31 (2001) 269–286.
[36] I. Marshall, J. Higinbotham, S. Bruce, A. Freise, Use of Voigt lineshape for quantification of in vivo ^{1}H spectra, Magn. Reson. Med. 37 (1997) 651–657.